Romanian Reports in Physics, Vol. 66, No. 4, P. 993–1001, 2014

AZO THIN FILMS SYNTHESIZED BY RF-MAGNETRON SPUTTERING: THE ROLE OF DEPOSITION POWER

Cristina BESLEAGA[1,2], L. ION[1], S. ANTOHE[1]

[1]University of Bucharest, Faculty of Physics, P.O. Box MG-11, RO-077125 Bucharest-Magurele, Romania
[2]National Institute of Materials Physics, P.O. Box MG-7, RO-077125 Magurele-Ilfov, Romania
E-mail address: santohe@solid.fizica.unibuc.ro

Received August 12, 2013

Abstract. Transparent *c-axis* textured aluminum doped zinc oxide (AZO) films were deposited at room temperature onto glass substrates by radio-frequency magnetron sputtering. The effect of sputtering power on the properties of the AZO sputtered thin films was investigated. Our results indicated that the sputtering power has a great influence on the crystalline quality and electrical parameters of AZO films, thus being a useful tool for tuning their functional properties.

Key words: AZO thin films, magnetron sputtering, XRD, band gap, electrical parameters.

1. INTRODUCTION

The transparent conducting oxide (TCO) thin films should have low resistivity, high transmittance in the visible region and high thermal/chemical stability. Achieving large conductivities in transparent oxides is challenging because of the complex interplay with the optical properties [1, 2]. Furthermore, the surface morphology of a TCO layer is of great importance, since the reliability and stability of all semiconductor devices is strongly dependent on the quality of TCO/semiconductor interfaces [3].

Today the most common TCO available on market is indium tin oxide (ITO), but in order to stay competitive and independent in the electronics industry, a large effort is invested in developing rare-metals-free TCO materials [4].

The TCOs based on zinc oxide (ZnO) are the most promising due to their remarkable electrical and optical properties [5–7]. In order to further improve the electrical conductivity of ZnO thin films, group III elements such as boron [8], gallium [9], or indium [10, 11], are usually used to dope ZnO and boost its functionality.

Aluminum-doped zinc oxide (AZO), represents a lower cost (due to its large earth-abundance and cheap extraction/production) and less toxic alternative to the previous mentioned ZnO-based TCO materials. Moreover, the AZO superiority in

terms of optical and electronic properties [5, 12] foresees its great future in electronics. AZO can be used in a wide range of applications, like transparent transistors [13, 14], photovoltaic cells [15, 16], gas sensors [17], or non-volatile memories [18].

It is therefore easy to understand the frantically search for reliable technological solutions able to produce high-quality AZO thin films. Obtaining high performance AZO films was attempted worldwide by using a variety of deposition methods including, pulsed laser deposition [12], ultrasonic spray pyrolysis [19], electrostatic spray deposition [20], chemical vapor deposition [21] or sol-gel [22]. A reliable deposition technique is radio-frequency magnetron sputtering (RF-MS), which allows the synthesis of pure, uniform, smooth, highly-adherent and self-sustainable thin films over large area substrates, as well as the easy scale-up process and efficient technological transfer to industry [23]. Hitherto, RF-MS has proven its remarkable potential in many types of high-tech applications in tribology [24, 25], telecommunications [26, 27], medicine [28, 29] or automotive and aerospace engineering [24, 30].

Here, a complete technological algorithm for fabricating AZO thin films is presented, starting with the preparation of a sputtering target of desired composition, continuing with the synthesis of AZO layers by RF-MS, and ending with a multi-parametrical analysis of the sputtered layers. The effect of sputtering power upon the structural, optical, morphological and electrical properties is put forward, and the optimal deposition conditions for preparing good quality AZO-based TCOs are highlighted.

2. EXPERIMENTAL

2.1. TARGET PREPARATION

High purity ZnO and α-Al_2O_3 powders (99.99%, Sigma Aldrich) were used to prepare the ceramic sputtering AZO target. The average particle sizes of ZnO and α-Al_2O_3 powders were 20–30 μm and 100 nm, respectively. For this study the chosen amount of Al_2O_3 doping was of 2.2 wt. %. The selected powder blend was thoroughly mixed by ball-milling (agate balls) with methanol for 1 hour. After this process the mixed slurry was calcined at 1100°C/5h to remove moisture, organic remnants, and to induce the decomposition of carbonates and other residual compounds. The resulted powder was deferred to a second ball-milling stage with methanol for 1h, the resulted slurry being dried in an oven at 200°C/24 hours. The dried powder was further mixed with polyvinyl alcohol and then the powder de-agglomerated by sieving through a 100 standard mesh.

In a final stage the resulted powder was pressed in an austenitic stainless steel die-pot (chamber dimensions: diameter = 60 mm, height = 4 mm) using a uniaxial pressure of 50 MPa. A three steps thermal treatment was applied to the AZO green

compact target: 100°C/4h - first plateau; 600°C/1 h – debinding and 1400°C/5h – sintering. A 2°C/min heating and cooling rate was used for sintering. The sintered compact, having a diameter of 50 mm and a thickness of 3 mm, was mechanical grinded down to a to 1000 grit SiC.

2.2. SUBSTRATES

UV grade glass slides (Fisher Scientific Microscope Slides) were used as substrates. Prior to deposition the substrates were ultrasonically cleaned in acetone and isopropyl alcohol for 10 minutes. The substrates were then dried in argon flow and fixed on the deposition system holder.

2.3. DEPOSITION PROCEDURE

A sputtering deposition system (13.56 GHz) was used to deposit the AZO thin films. The deposition chamber, was first evacuated to a pressure $\sim 2\times10^{-3}$ Pa, and then, spectral argon was admitted up to a 0.4 Pa (sputtering) pressure. The AZO films were prepared at room temperature, using a target-to-substrate distance of 60 mm. The sputtering of the AZO thin films was carried out at four constant cathode powers (30, 60, 100 and 150 W), in order to evaluate the influence of this sputtering variable on the physical properties of AZO films. The samples will be further denoted: S1 (30 W), S2 (60 W), S4 (100 W), and S4 (150 W).

2.4. CHARACTERIZATION TECHNIQUES

i) The crystalline status of the target and deposited films was investigated with a Bruker D8 Advance X-ray diffractometer, using Cu K_α radiation and a high efficiency linear detector of LynxEye type. The XRD measurements were performed in symmetric (θ-θ) geometry, the scattered intensity being scanned in the 20–80° (2θ) range, with a step size of 0.04°, and 6s acquisition time per step.

ii) The films' thicknesses were determined by X-ray reflectivity and optical measurements.

iii) The optical transmission analyses were carried out using a UV-VIS Perkin-Elmer Lambda 35 Spectrophotometer.

iv) The morphological features of the AZO thin films were examined by an A100-AFM microscope working in the non-contact mode in air at a 325 kHz resonance frequency and a ~46 N/m constant force, equipped with a commercial silicon cantilever. AFM micrographs were recorded from different regions of the samples, using sampling areas of 3×3 μm^2.

v) The electrical measurements were performed at room temperature, below 10^{-2} Pa pressure, with a Keithley 2400 source-meter and a Keithley 6517 electrometer, using Van der Pauw geometry.

3. RESULTS AND DISCUSSION

3.1. STRUCTURAL PROPERTIES OF AZO THIN FILMS

XRD analyses have been performed first on the as-prepared AZO target (Fig. 1a). The XRD pattern revealed that the target consisted of a majority hexagonal ZnO phase (ICDD: 01–089–0510), with sharp prominent peaks, and a minority gahnite ($ZnAl_2O_4$) phase (ICDD: 01–070–8181), displaying less intense diffraction lines.

The XRD measurements of the sputtered AZO films (Fig. 1b,c,d) indicated, irrespective of deposition power, their monophasic ZnO wurtzite structure (ICDD: 01–089–0510) with relatively good crystallinity. All the films showed a <*00l*> preferential orientation (Fig. 1c).

Deviations of the diffraction peaks toward lower angles with respect to the bulk AZO were noticed (Fig. 1c,d), and might be attributed to the imperfect stoichiometry, non-isometric deposition of the crystallites and/or to the presence of a uniform tensile stress.

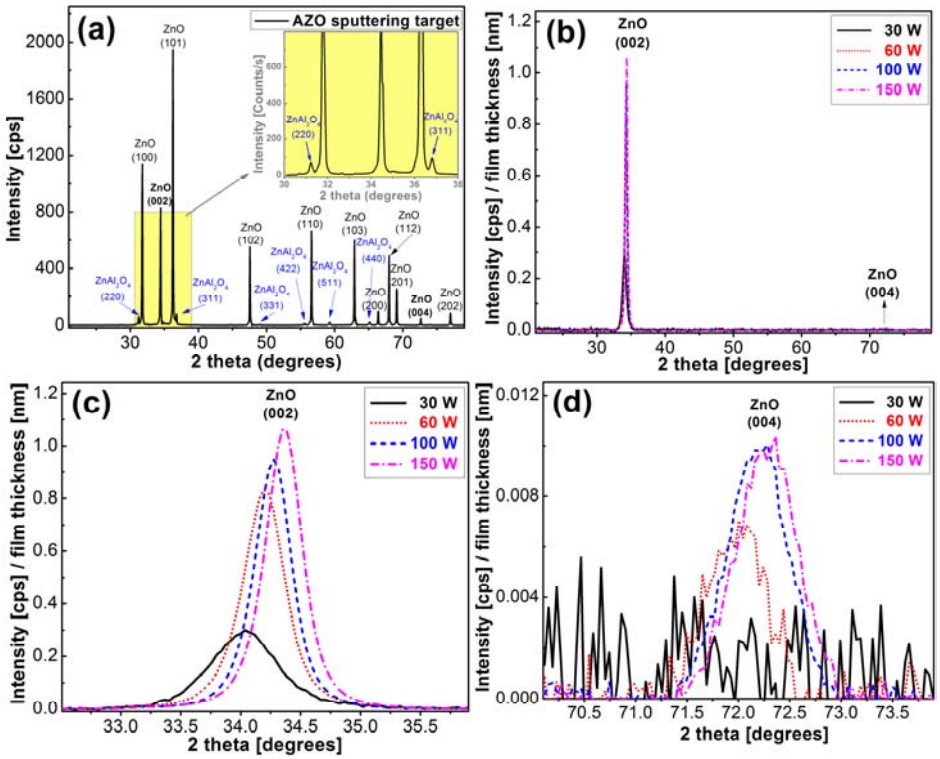

Fig. 1 – Comparative X-ray diffraction patterns for: a) AZO target; b) AZO sputtered films; c) 002 peak region detail; d) 004 peak region detail for the AZO films.

The effective size of coherent zones on [001] direction were determined using Scherrer equation (Table 1). One can notice that the films' crystallinity increases with the sputtering power (Table 1 and Fig. 1c). When the sputtering power is increased, the energy of the sputtered species is augmented, and grain sizes become larger due to the enhanced surface diffusion of the ad-atoms.

Table 1

Important structural and optical features of AZO thin films: 002 peaks' position (2θ), effective sizes (D_{eff}) of coherent zone on [001] direction extracted using the Scherrer equation, and band gap values

Sample code	Cathode power [W]	Max. (002) peak 2θ [deg.]	D_{eff} (002) [nm]	E_g [eV]
Target	-	34.449	-	-
S1	30	34.003	11.5	3.6
S2	60	34.173	17.7	3.5
S3	100	34.248	20.1	3.4
S4	150	34.339	20.4	3.3

3.2. OPTICAL PROPERTIES OF AZO FILMS

The transmission spectra of the prepared samples are presented in Fig. 2, showing transmittance values of about 80%, for all the AZO layers. The band gap values are presented in Table 1. One can also notice that the E_g values monotonously decreased with the increase of the effective size of crystalline coherent zone (Table 1), and hence with the increase of the sputtering power.

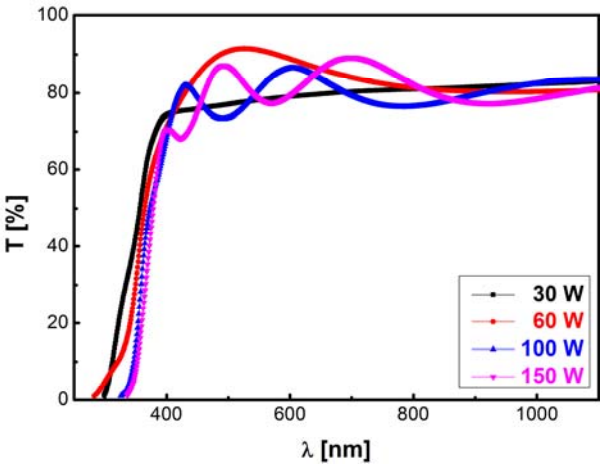

Fig. 2 – Transmission spectra for the AZO films sputtered at different cathode powers.

3.3. MORPHOLOGICAL FEATURES OF AZO FILMS

Typical AFM micrographs for the AZO thin films are presented in Fig. 3. One can observe an increase of AZO grains size and uniformity (S3, S4) with the sputtering power.

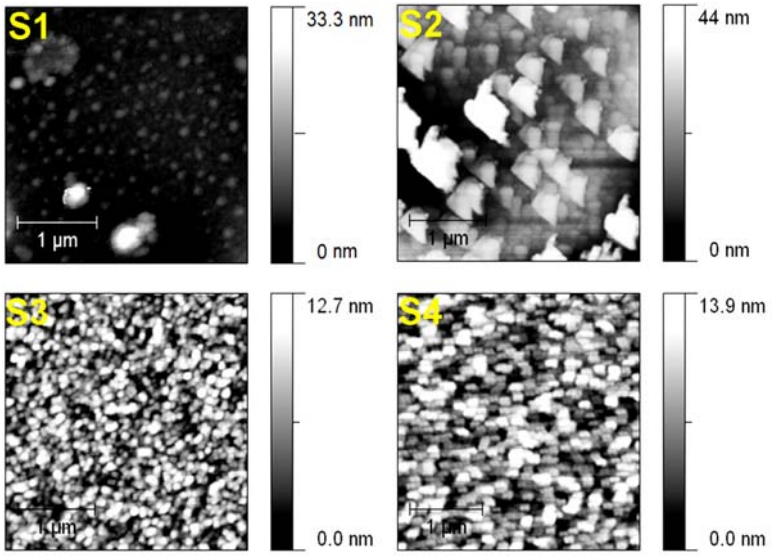

Fig. 3 – Morphology dependence of AZO films on sputtering power, as revealed by the AFM analyses.

Statistical surface parameters of the AZO films, such as surface roughness, surface skewness (S_{sk}) and surface kurtosis (S_{ku}), are collected in Table 2. The films' roughness values are relatively small, ranging from 2 nm to 10 nm, and are rather typical for magnetron sputtering films deposited at room temperature. For all the analyzed samples, the S_{sk} parameter (indicator of asymmetry and deviation from a normal distribution) exhibited positive values, greater than 1, whilst the S_{ku} values (a measure of "peakedness") are higher than 3, suggesting that the surfaces of the AZO films are flat with extreme peaks (grains) having a sharp distribution of heights.

Table 2

AFM statistical parameters for the AZO thin films

Sample code	Cathode Power [W]	Roughness (RMS) [nm]	S_{sk}	S_{ku}
S1	30	2.5	1.7	4
S2	60	7.3	2.7	9.0
S3	100	2	5.2	56.4
S4	150	10	3.9	18.7

3.4. ELECTRICAL PROPERTIES OF AZO FILMS

The dependence of the electrical resistivity (ρ), mobility (μ) and carrier concentration (n) of AZO films on the sputtering power is shown in Fig. 4. A linear dependence of the electronic mobility and resistivity of AZO layers on their crystalline quality (Fig. 1b,c,d) can be depicted. The increase of the free carriers' mobility together with the significant decrease of the resistivity can be related to the reduction of the grain boundaries effect which plays an important role in charge trapping and scattering in oxide materials [31]. The AZO film deposited at 150 W exhibited best TCO electric properties, having an electric resistivity of 1.49×10^{-2} Ωcm and a charge mobility of 7.7 cm^2/Vs. These values are superior to the ones recently reported by Jun *et al.* [32].

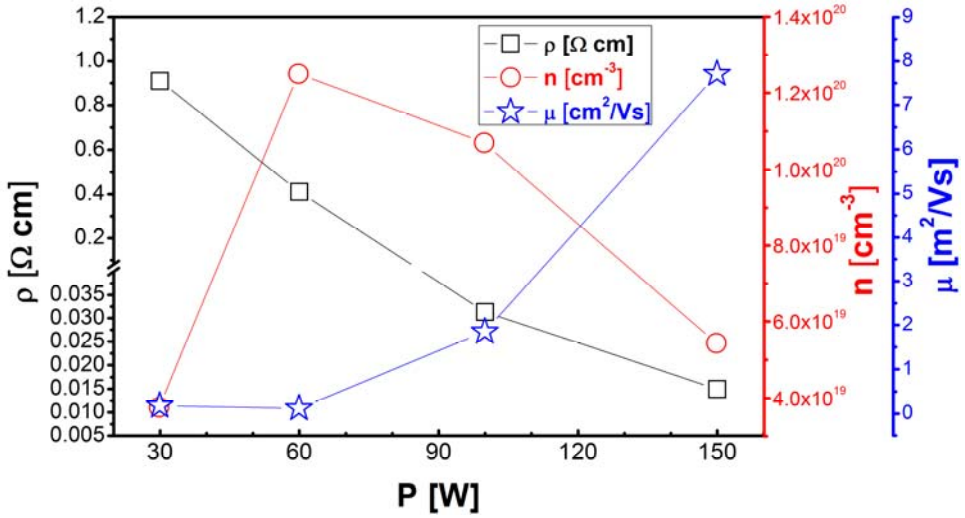

Fig. 4 – The AZO films' electrical resistivity (ρ), mobility (μ) and carrier concentration (*n*) function of the sputtering power.

The evolution of the AZO free carriers' density with the deposition power is not linear, as was the case of the resistivity or the electronic mobility (Fig. 4). This can be intuitively attributed to an energetic threshold necessary for the Al atoms to be substitutionally integrated in the ZnO crystalline lattice.

Yang *et al.* [33] indicated that when using a low power regime, most Al atoms would segregate to non-crystalline regions, at grain boundaries, forming Al–O bonds. Thus, the formation of various Al_xO_y compounds, which can be considered an ineffective doping, is more plausible in these conditions. This is due to the higher binding energy of the Al–O bond (511 ± 3 kJ/mol) than that of Zn–O bond (159 ± 4 kJ/mol), and to the lower free energy of formation (ΔG_f) of Al_2O_3 (−1582.3 kJ/mol) as compared to that of ZnO (−320.5 kJ/mol) [34, 35]. However,

when increasing the working power the bombarding argon ions attain higher energies, being able to break more easily the Al_2O_3 or $ZnAl_2O_4$ (gahnite) molecules from the target, and deliver more efficiently Al donors to the growing film. With higher deposition power, the energy of the arriving Al ad-atoms gets sufficient for entering the ZnO lattice as substitutionals, which can explain the significant increase of free carrier concentration, when the sputtering power is raised from 30 to 60 W.

The decrease of the free carrier density, observed for the AZO layers deposited at powers higher than 60 W, can by linked with a progressive reduction of the oxygen vacations due to the ability of the now more energetic ad-atoms to transversally diffuse into convenient energy sites, instead of frozen in their arriving sites, thus increasing the ZnO-matrix ordering.

The AZO carrier density value, corresponding to the larger mobility value (S4), is 5.4×10^{19} cm^{-3}, being in good agreement with the literature [36, 37].

4. CONCLUSIONS

c-axis textured aluminum-doped zinc oxide thin films were successfully fabricated by RF-magnetron sputtering at room temperature, using a lab-prepared ceramic AZO target having a 2.2 wt.% aluminum doping. All the AZO films presented good optical transparency in visible range (~80%), resistivity values lower than 0.9 Ωcm, and charge mobility values up to 7.7 cm^2/Vs. The free carrier mobility and conductivity values increased with the crystalline quality of the AZO layers. Our study showed that the electrical parameters of the AZO films are dependent on their structural properties, which in turn can be easily controlled by the sputtering cathode power variation.

Acknowledgements. C.B. is grateful for financial support from the ESF through POSDRU107/1.5/S/80765 project.

REFERENCES

1. L. Castañeda, Materials Science and Applications, **2**, 1233–1242 (2011).
2. H. Liu, V. Avrutin, N. Izyumskaya, Ü. Özgür, and H. Morkoç, Superlattices and Microstructures, **48**, 458–484 (2010).
3. K. Jäger, M. Fischer, R. A. C. M. M. van Swaaij, and M. Zeman, J. Appl. Phys., **111**, 083108 (2012).
4. T. Minami, Thin Solid Films, **516**, 5822–5828 (2008).
5. A. Stadler, Materials, **5**, 661–683 (2012).
6. C. Besleaga, G. E. Stan, A. C. Galca, L. Ion, and S. Antohe, Appl. Surf. Sci., **258**, 8819–8824 (2012).
7. M. Nistor, Rom. Rep. Phys., Suppl., **64**, 1313–1322 (2012).

8. H. Zhu, Y. Feng, L. Zhang, B. Lai, T. He, D. Liu, Y. Wang, J. Yin, Y. Ma, Y. Huang, H. Jia, and Y. Mai, Physica Status Solidi **(a)**, **209**, 1259–1265 (2012).
9. V. Bhosle, J. T. Prater, Fan Yang, D. Burk, S. R. Forrest, and J. Narayan, J. Appl. Phys., **102**, 023501 (2007).
10. G. Socol, D. Craciun, I. N. Mihailescu, N. Stefan, C. Besleaga, L. Ion, S. Antohe, K. W. Kim, D. Norton, S. J. Pearton, A. C. Galca, and V. Craciun, Thin Solid Films, **520**, 1274–1277 (2011).
11. C. Besleaga, L. Ion, V. Ghenescu, G. Socol, A. Radu, I. Arghir, C. Florica, and S. Antohe, Thin Solid Films, **520**, 6803–6806 (2012).
12. A. C. Galca, M. Secu, A. Vlad, and J. D. Pedarnig, Thin Solid Films, **518**, 4603–4606 (2010).
13. P. Ray, V. Ramgopal Rao, Appl. Phys. Lett., **102**, 064101 (2013).
14. Y. S. Park, H.-K. Kim, Thin Solid Films, **519**, 8018–8022 (2011).
15. M. L. Grilli, A. Sytchkova, S. Boycheva, and A. Piegari, Physica Status Solidi **(a), 210**, 748–754 (2013).
16. S.-H. Lee, S.-H. Han, H. S. Jung, H. Shin, J. Lee, J.-H. Noh, S. Lee, I.-S. Cho, J.-K. Lee, J. Kim, and H. Shin, J. Phys. Chem. **C, 114**, 7185–7189 (2010).
17. I. G. Dimitrov, A. O. Dikovska, P. A. Atanasov, T. R. Stoyanchov, and T. Vasilev, J. Phys.: Conf. Ser., **113**, 012044 (2008).
18. D. Lee, D.-K. Hwang, M. Chang, Y. So, D.-J. Seong, D. Choi, and H. Hwang, Non-Volatile Semiconductor Memory Workshop, IEEE NVSMW 21st, 2006, pp. 86–87.
19. R. Pandey, S. Yuldashev, H. D. Nguyen, H. C. Jeon, and T. W. Kang, Current Applied Physics, **12**, S56–S58 (2012).
20. K. Mahmood, S. B. Park, Electron. Mater. Lett., **9**, 161–170 (2013).
21. W.-H. Kim, W. J. Maeng, M.-K. Kim, and H. Kim, J. Electrochem. Soc., **158**, D495–D499 (2011).
22. E. Vasile, S. Mihaiu, R. Plugaru, Dig. J. Nanomater. Biostr., **8**, 721–727 (2013).
23. K. Wasa, M. Kitabatake, and H. Adachi, *Thin Film Materials Technology: Sputtering of Compound Materials*, Springer-Verlag, Heidelberg, 2004.
24. P. J Kelly, R .D. Arnell, Vacuum, **56**, 159–172 (2000).
25. Q. Yang, L. R. Zhao, P. C. Patnaik, and X. T. Zeng, Wear, **261**, 119–125 (2006).
26. H. Okano, N. Tanaka, Y. Takahashi, T. Tanaka, K. Shibata, and S. Nakano, Appl. Phys. Lett., **64**, 166 (1994).
27. D. Neculoiu, A. Müller, G. Deligeorgis, A. Dinescu, A. Stavrinidis, D. Vasilache, A.M. Cismaru, G.E. Stan, G. Konstantinidis, Electron Lett., **45**, 1196–1197 (2009).
28. Y. Yang, K.-H. Kim, and J. L. Ong, Biomaterials, **26**, 327–337 (2005).
29. G. E. Stan, J. Optoelectron. Adv. Mater., **11**, 1132–1138 (2009).
30. H. Altun, S. Sen, Surf. Coat. Technol., **197**, 193–200 (2005).
31. D. H. Zhang, H. L. Ma, Appl. Phys. A, **62**, 487–492 (1996).
32. M.-C. Jun, S.-U. Park, and J.-H. Koh, Nanoscale Res. Lett., **7**, 639 (2012).
33. W. Yang, Z. Liu, D. L. Peng, F. Zhang, H. Huang, Y. Xie, and Z. Wu, Appl. Surf. Sci., **255**, 5669–5673 (2009).
34. K.-K. Kim, S. Niki, J.-Y. Oh, J.-O. Song, T.-Y. Seong, S.-J. Park, S. Fujita, and S.-W. Kim, J.Appl. Phys., **97**, 066103 (2005).
35. G. Yu, Y. Liu, D. Hong, D. Li and J. Zang, Adv. Mater. Res., **557-559**, 1945–1949 (2012).
36. S. Mridha, D Basak, J. Phys. D: Appl. Phys., **40**, 6902 (2007).
37. M. Mozibur Rahman, M. K. R. Khan, M. Rafiqul Islam, M. A. Halim, M. Shahjahan, M. A. Hakim, D. K. Saha, and J. U. Khan, Mater. Sci. Tehnol., **28**, 329–335 (2012).